Published in final edited form as:
Channels (Austin). 2009 November ; 3(6): 448–461.

A Novel N-terminal Motif of Dipeptidyl Peptidase-like Proteins Produces Rapid Inactivation of Kv4.2 Channels by a Pore-blocking Mechanism

Henry H. Jerng[1], **Kevin Dougherty**[2], **Manuel Covarrubias**[2], and **Paul J. Pfaffinger**[1]

[1] Department of Neuroscience, Baylor College of Medicine, Houston, TX 77030

[2] Department of Pathology, Anatomy, and Cell Biology, Jefferson Medical College of Thomas Jefferson University, Philadelphia, PA 19107

Abstract

The somatodendritic subthreshold A-type K^+ current in neurons (I_{SA}) depends on its kinetic and voltage-dependent properties to regulate membrane excitability, action potential repetitive firing, and signal integration. Key functional properties of the Kv4 channel complex underlying I_{SA} are determined by dipeptidyl peptidase-like proteins known as dipeptidyl peptidase 6 (DPP6) and dipeptidyl peptidase 10 (DPP10). Among the multiple known DPP10 isoforms with alternative N-terminal sequences, DPP10a confers exceptionally fast inactivation to Kv4.2 channels. To elucidate the molecular basis of this fast inactivation, we investigated the structure-function relationship of the DPP10a N-terminal region and its interaction with the Kv4.2 channel. Here, we show that DPP10a shares a conserved N-terminal sequence (MNQTA) with DPP6a (aka DPP6-E), which also induces fast inactivation. Deletion of the NQTA sequence in DPP10a eliminates this dramatic fast inactivation, and perfusion of MNQTA peptide to the cytoplasmic face of inside-out patches inhibits the Kv4.2 current. DPP10a-induced fast inactivation exhibits competitive interactions with internally applied tetraethylammonium (TEA), and elevating the external K^+ concentration accelerates recovery from DPP10a-mediated fast inactivation. These results suggest that fast inactivation induced by DPP10a or DPP6a is mediated by a common N-terminal inactivation motif via a pore-blocking mechanism. This mechanism may offer an attractive target for novel pharmacological interventions directed at impairing I_{SA} inactivation and reducing neuronal excitability.

Keywords

DPP6; DPP10; auxiliary subunits; inactivation; Kv4 channels

INTRODUCTION

Voltage-activated potassium channels belonging to the Kv4 subfamily (Kv4 channels) underlie the somatodendritic subthreshold A-type current (I_{SA}) that regulates membrane excitability, action potential firing frequency, action potential backpropagation, and synaptic plasticity in neurons.[1], [2] In the native I_{SA} channel, the Kv4 pore-forming subunits form heteromultimeric assemblies with diverse auxiliary subunits including Kv channel-interacting proteins (KChIP1-4) and dipeptidyl peptidase-like proteins (DPLP: DPP6/DPPX and DPP10/DPPY).[1], [3], [4] Individually, KChIP and DPLP auxiliary subunits dramatically

Corresponding author: Henry H. Jerng, Department of Neuroscience, Baylor College of Medicine, One Baylor Plaza, S630, Houston, TX 77030, Tel.: (713) 798-3062, Fax: (713) 798-3946, hjerng@cns.bcm.tmc.edu.

modify Kv4 channel surface expression, kinetics, and voltage-dependent properties.[5–8] Together in Kv4+KChIP+DPLP ternary complexes, these auxiliary subunits finely tune the Kv4 channel machinery to determine the native I_{SA} functional properties.[6, 9, 10]

Heteromultimeric assembly of multiple subunit classes (KChIP and DPLP) and multiple gene products (KChIP1-4, DPP10 and DPP6) has been proposed as a major source of variability in I_{SA} biophysical properties observed between different neuronal cell-types and populations.[1] However, recent reports suggest that N-terminal variants generated by alternative splicing may also be critical determinants of cell-specific I_{SA} properties. The genes for both KChIP and DPLP subunits utilize multiple promoter sites, producing alternative transcripts with variable N-terminal domains and an invariable core domain.[1, 11–14] The resulting isoforms exhibit distinct tissue- and cell-specific expression patterns in the brain and may confer unique gating properties. A remarkable example is the DPP10a isoform, which confers dominant fast inactivation ($\tau \leq 10$ ms) to the Kv4 complex.[11] Since DPP10a is typically expressed in cortical neurons, co-expression of Kv4.2, KChIP3a, and DPP10a in heterologous expression systems induces a rapidly inactivating K^+ current that recapitulates cortical I_{SA}.

How does DPP10a confer this dominant fast inactivation of Kv4 channels? The variant-specific nature of this fast inactivation suggests that the responsible molecular determinant is located in the DPP10a variable N-terminal segment. In agreement with an N-terminal involvement, our initial characterization of DPP10a demonstrated that DPP10a-mediated fast inactivation is inhibited by N-terminal tagging of a hemagglutinin epitope and transferrable to the DPP6-S isoform by switching the DPP6-S variable N-terminal domain for that of DPP10a.[7] We therefore hypothesized that the fast inactivation mediated by the DPP10a N-terminal domain may be similar to the classic N-type inactivation mechanism first described in Shaker K^+ channels. N-type inactivation occurs when a channel opens in response to strong depolarization and an N-terminal inactivation domain (ID) occludes the channel pore from the cytoplasmic side.[15] IDs for such open-channel block are found at the N-termini of certain Shaker α-subunits, Shaker-related Kv1.4 α-subunits, Kv3.4 α-subunits, and Kv1 auxiliary Kvβ subunits.[15–18] The N-terminus of Kv4.2 α-subunits also possesses an ID that causes channel block similar to Shaker N-type inactivation, although with distinct structural determinants.[19] Since N-type inactivation is produced by internal pore block, the standard criteria for this mechanism are 1) competition between TEA, a fast open-channel blocker, and the ID for the occlusion site, and 2) a “knock-off” effect induced by elevated external K^+ concentrations during recovery from inactivation. [20, 21] Although a role for the cytoplasmic N-terminal domain in DPP10a-mediated fast inactivation is hinted by our previous results, the molecular basis of these effects remained unknown. Here, we establish the importance of the Exon 1a-encoded N-terminal domain for DPP10a-mediated fast inactivation by characterizing a DPP6 paralog of DPP10a. DPP6a (aka DPP6-E) is expressed from an alterative first exon of the DPP6 gene, one in a homologous position to Exon 1a of the DPP10 gene. Both Exon 1a’s of DPP6 and DPP10 encode an evolutionarily preserved N-terminal sequence (MNQTA). Using deletion and individual point mutants, we demonstrate that the MNQTA motif is critical for the induction of fast inactivation. Further results show that fast inactivation induced by MNQTA is competed off by internal TEA and is relieved by elevated external K^+ concentration, which is consistent with an open-channel-block mechanism. Part of this study was previously reported in preliminary form elsewhere.[22]

RESULTS

DPP6a is a paralog of DPP10a with homologous N-terminal sequences

We have previously shown that the DPP10 gene encodes multiple transcripts with alternative start sites, and the transcript beginning with Exon 1a codes for DPP10a, the isoform that confers uniquely fast inactivation to Kv4 channels.[11] The DPP6 gene also expresses different first exon variants due to initiation from various start sites, and recently we and others have shown that a DPP6 isoform expressed in embryos also produces fast inactivation.[10, 22, 23] This DPP6 isoform, which we named DPP6a due to its similarity to DPP10a, contains an N-terminal domain with significant sequence homology to the N-terminal domain of DPP10a (Fig. 1A). The N-terminal domains encoded by Exon 1a of DPP10a and DPP6a are the same length (20 amino acids) and share identical first five residues. These first five residues, MNQTA, are preserved evolutionarily from fish and amphibians to humans and are likely part of an important functional domain. In addition, lysine 17 and 20 are also identical between DPP10a and DPP6a.

Since DPP10 and DPP6 genes have significant sequence identity (51%) and are likely paralogs derived from gene duplication, we examined the genomic organizations of the alternative first exons to study the possible paralogous relationship between DPP6a and DPP10a. Genomic mapping demonstrates that Exon 1s of DPP10a and DPP6a are the most 5′-upstrem of alternative first Exons (Fig. 1B). DPP10 alternative first exons are scattered across approximately half a million base pairs and cover more than 60% of the gene's total length. These exons are present in other mammalian genomes and are also found in ESTs from a number of mammalian and non-mammalian species. The overall DPP6 genomic structure is strikingly similar to that described for DPP10 where multiple first exons are scattered over 900,000 base pairs and cover over 60% of the genes total length. The sequence homology and genomic localization suggests that DPP6a is a paralog of DPP10a.

DPP10a and DPP6a Confers Similar Fast Inactivation to the Kv4.2+KChIP3a Channel

To determine the extent by which similar N-terminal sequences between DPP10a and DPP6a translate into similar functional effects in the reconstituted ternary channel complex, we co-expressed Kv4.2 and KChIP3a with either DPP10a or DPP6a in *Xenopus* oocytes and recorded the resulting whole-cell currents. Co-expression with KChIP3a permits convenient detection of DPP10a-mediated fast inactivation by eliminating endogenous Kv4.2 fast inactivation through KChIP-mediated sequestration of Kv4.2 N-terminal domain.[1, 19, 24] Kv4.2 and KChIP3a were also co-expressed with DPP6-S (short) as a control for effects derived from the DPP6 invariable core domain.

During a sustained depolarization to positive membrane potentials, ternary channel complexes containing DPP10a and DPP6a decay rapidly with similar complex multi-exponential time course (Fig. 2A).[9] At membrane potentials at or above −20 mV, at least three time constants are necessary to adequately describe the current decay elicited by 1- or 5-sec step depolarizations to various potentials from a holding potential of −100 mV (Fig. 2A; compare the residuals of two exponential fits against that of three exponential fits for Kv4.2+KChIP3a+DPP10a current at +50 mV). For display purposes, Figure 2A shows current traces for the initial 330 ms. The three time constants of exponential terms 0 ($\tau 0$) and 1 ($\tau 1$) are weakly voltage dependent from −20 to +50 mV, whereas the time constant of exponential term 2 ($\tau 2$) significantly increased with increasing depolarization (not shown). Fit parameters were independent of peak current size between 1 and 30 μA, indicating current decay is not significantly affected by uncompensated series resistance. Similar results were obtained previously for Kv4.2+KChIP3a+DPP10a channels in whole-cell patch recording from CHO cells.[9] The results of tri-exponential fittings show that the fast phase of

inactivation accounts for > 60% of total inactivation in these channels and decays with similar time courses (τ0: Kv4.2+KChIP3a+DPP10a = 6.5 ± 0.4 ms, n=6; Kv4.2+KChIP3a +DPP6a = 5.9 ± 0.1 ms, n=4) (Fig. 2B & 2C). In addition, the slow phase also inactivates with similar time constants (τ2: Kv4.2+KChIP3a+DPP10a = 615 ± 40 ms, n=6; Kv4.2+KChIP3a+DPP6a = 582 ± 41 ms, n=4) but accounts for different fraction of the total inactivation (Fig. 2B & 2C).

In contrast, Kv4.2+KChIP3a+DPP6-S current decay is well described assuming the sum of two exponential terms (Fig. 2A; compare the residuals of one exponential fits against that of two exponential fits). The same currents heterologously expressed in CHO cells were also adequately described using two exponential terms.[9] Co-expression of KChIP3a with Kv4.2 also inactivates with a bi-exponential decay (Fig. 2B), showing that DPP6-S, unlike DPP6a and DPP10a, does not introduce a fast phase of inactivation. The time constants of the fast phase of inactivation of Kv4.2+KChIP3a and Kv4.2+KChIP3a+DPP6-S channels at +50 mV are similar to that of the intermediate inactivation of Kv4.2+KChIP3a+DPP10a channels (τ1), suggesting that the fast inactivation (τ = ~ 6 ms) conferred by DPP10a and DPP6a is introduced by the presence of the conserved N-terminal domain. Furthermore, the presence of this conserved N-terminal inactivation domain is associated with a pronounced slowing of the slow phase of inactivation, increasing the time constant (τ2) from ~ 180 ms (Kv4.2+KChIP3a+DPP6-S) or 187 (Kv4.2+KChIP3a) ms to ~600 ms (Fig. 2B).

Although DPP6a and DPP10a produce similar effects on the development of voltage-dependence of inactivation, the rate of accelerated recovery from inactivation induced by DPP6a is faster than that induced by DPP10a (τ at −100 mV: Kv4.2+KChIP3a+DPP6a = 10.3 ± 0.3 ms, n=3; Kv4.2+KChIP3a+DPP10a = 28 ± 3.5 ms, n=7) (Fig. 2D). The faster recovery induced by DPP6a is not a property of DPP6 in general, since it is faster than that induced by DPP6-S (Fig. 2D). Similar results were obtained from DPP6a and DPP10a coexpression studies using an N-terminal deletion of Kv4.2 (Kv4.2/Δ2-40), showing that the regulatory effects are not mediated through KChIPs (data not shown). These findings suggest that amino acid differences between the Exon 1a of DPP10a and DPP6a account for the faster recovery from inactivation of channels coexpressed with DPP6a.

To examine whether the differential effects on inactivation kinetics can be related to changes in voltage-dependent gating, we characterized the voltage dependence of peak conductance and steady-state inactivation and found that Kv4.2+KChIP3a channels associated with DPP6a, DPP10a, or DPP6-S show similar relations (Fig. 2E). The peak conductance-voltage (Gp-V) curves were all well described by a 4th-order Boltzmann function with $V_{0.5}$ values between −19 and −21 mV and slope values between 20 and 23 mV. The steady-state inactivation curves were fitted with single Boltzmann functions with $V_{0.5}$ values at ~ −68 mV and slope factors between 4.4 and 5 mV. This indicates that putative N-terminal domains in DPP6a and DPP10a do not affect peak activation or steady-state inactivation differently from DPP6-S N-terminal domain, and the inactivation-inducing effect of DPP6a and DPP10a N-terminal domains likely occurs without altering other gating properties.

The MNQTA N-terminal Sequence in DPP10a Confers Fast Inactivation

So far, our results suggest that DPP10a and DPP6a utilize a common mechanism to induce a dominant fast inactivation in Kv4 channels. To identify the molecular determinants of fast inactivation, we focused on DPP10a and generated DPP10a mutants lacking Exon 1a (Δ2-20) or residues 2-5 (ΔNQTA). Instead of Kv4.2+KChIP3a channels, we used Kv4.2/Δ2-40 channels to test these mutants because they exhibit many of the same functional characteristics due to the similar structural impact between N-terminal deletion and KChIP-mediated sequestration,[11] and their use alleviates concerns over potential heterogeneity in channel composition arising from Kv4.2-KChIP coexpression and coassembly.

Coexpression of Kv4.2/Δ2-40 with DPP10a/Δ2-20 results in a current that activates rapidly but inactivates with a time course dramatically slower than that of Kv4.2/Δ2-40+DPP10a channels (Figs. 3A). Moreover, deletion of DPP10a residues NQTA is sufficient to abolish the ability of DPP10a to confer fast inactivation (Fig. 3B). Exponential fitting was used to measure the inactivation of Kv4.2/Δ2-40 channels co-expressed with DPP10a, DPP10a/Δ2-20, or DPP10a/ΔNQTA at +50 mV. Evaluation of the residual current between the fit and actual traces (as conducted in Fig. 2A) shows that the sum of three exponential terms is necessary to describe the inactivation of Kv4.2/Δ2-40+DPP10a current at +50 mV, whereas the sum of two exponential terms is sufficient to describe currents modified by DPP10a deletion mutants (see Fig. 3A & 3B residuals). The results show that, although DPP10a induces a fast inactivating component, the fast time constant Kv4.2/Δ2-40+DPP10a inactivation (3.2 ± 0.5 ms, n=3) differs by ~3 ms from that of the Kv4.2+KChIP3a+DPP10a inactivation (6.5 ± 0.4 ms, n=6) (compare Figs. 3C and 2B). N-terminal deletions of residues 2-20 or NQTA result in inactivation kinetics without a fast component of inactivation comparable to that observed in Kv4.2/Δ2-40+DPP10a channels (Fig. 3C). In addition, these deletions lead to a dramatic increase in the fractional contribution of the slow phase of inactivation and a marked acceleration of its kinetics (Fig. 3C & 3D). The time constants of the slow phase (τ2) decreased in value from 699 ± 28 ms (n=3) to 148 ± 3 ms (DPP10a/Δ2-20, n=4) and 170 ± 6 ms (DPP10a/ΔNQTA, n=6), and its fractional amplitude increased from ~ 0.09 to > 0.83. The acceleration of slow inactivation by N-terminal deletions is consistent with the earlier result showing that introduction of the fast inactivation impairs slow inactivation.

To verify that the failure of these deletion mutants to induce fast inactivation is not due to a loss or impairment of interaction with the Kv4.2 subunit, we checked other biophysical properties of these channels. Wild-type DPP10a and mutant DPP10a produce similar leftward shifts in the midpoint of steady-state inactivation ($V_{0.5}$: Kv4.2/Δ2-40 = −62 ± 1 mV, n=8; +DPP10a = −70 ± 1 mV, n=5; +DPP10a/Δ2-20 = −72 ± 0.3 mV, n=4; +DPP10a/ΔNQTA = −72 ± 0.4 mV, n=5). The amount of leftward shift in the midpoint of Gp-V relationship is ~15 mV less with DPP10a ($V_{0.5}$: Kv4.2/Δ2-40 = −1.3 ± 2 mV, n=5; +DPP10a = −19.7 ± 2 mV, n=5; +DPP10a/Δ2-20 = −34 ± 1 mV, n=4; +DPP10a/ΔNQTA = −36 ± 1 mV, n=4) (Figs. 3E & 3F) and is likely due to fast inactivation truncating the measured peak current and resulting in a shallower Kv.2/Δ2-40+DPP10a activation curve. Both DPP10a/Δ2-20 and DPP10a/ΔNQTA matched wild-type DPP10a in its functional effects on Kv4.2 activation kinetics (Fig. 3B, inset). Both deletion mutants accelerate recovery from inactivation similar to the wild-type DPP10a (τ at −100 mV: Kv4.2/Δ2-40 = 167 ± 19 ms, n=5; +DPP10a = 42 ± 1 ms, n=4; +DPP10a/Δ2-20 = 45 ± 2 ms, n=4; +DPP10a/ΔNQTA = 52 ± 3 ms, n=5). Overall, the results suggest that the deletions do not affect Kv4.2-DPP10 interactions with the voltage sensor.[8, 25]

Finally, we expressed Kv4.2/Δ2-40 channels with wild-type DPP10a or DPP10a/ΔNQTA subunits in mammalian tsA-201 cells and recorded the resulting currents in the cell-attached patch configuration. In agreement with the *Xenopus* oocyte data, Kv4.2/Δ2-40+DPP10a channels expressed in tsA-201 cells exhibit distinct fast inactivation (Fig. 4A), and when residues 2-5 of DPP10a are deleted, channel inactivation is greatly slowed (Fig. 4B & 4C). The slowing of inactivation is not due to a failure of DPP10a/ΔNQTA to associate with and modulate Kv4.2 channels, as the activation of Kv4.2+DPP10a/ΔNQTA current is equally rapid as Kv4.2+DPP10a current (Fig. 4C, inset). Collectively, the experiments in oocytes and tsA-201 cells produced compelling evidence of fast inactivation determined by a discrete five-amino acid N-terminal motif that is highly conserved in DPP10a and DPP6a.

Fast Inactivation Induced by DPP10a Is Constrained Specifically by the MNQTA Sequence

The MNQTA sequence is found at the N-terminus of DPP10a and DPP6a from fish to humans, and this sequence confers fast inactivation. To examine whether the ability to confer fast inactivation is sequence-specific, as suggested by the evolutionary preservation, we introduced conservative substitutions at positions 2–4 (NQTA) individually and studied their effects electrophysiologically upon coexpression with Kv4.2/Δ2-40. According to Venn diagram representing the physico-chemical relationships between amino acids,[26] asparagine (N), glutamine (Q), and threonine (T) are small polar residues, thus asparagine at position 2 was replaced by threonine (N2T), glutamine at position 3 was replaced by asparagine (Q3N), and threonine at position 4 was replaced by asparagine (T4N). Alanine at position 5, a small hydrophobic residue, is replaced by glycine (A5G), a small non-polar residue.

The results show that fast inactivation is sensitive to even small conservative substitutions with the NQTA sequence. The N2T mutant fails to induce fast inactivation (Fig. 5A). At +50 mV, inactivation kinetics of Kv4.2/Δ2-40+N2T channels is adequately described using two-exponential fitting, with time constants of 49 ± 2.3 ms and 211 ± 2.8 ms with respective fractional amplitudes of 0.16 ± 0.01 and 0.81 ± 0.01 (n=3). In contrast to N2T, the Q3N, T4N, and A5G substitution mutants confer varying amount of fast inactivation to Kv4.2/Δ2-40 channels. The current decay associated with Q3N coexpression is biphasic (rather than triphasic, as with wild-type DPP10a), and the fast component exhibits a time constant of 5.1 ± 0.5 ms and fractional amplitude of 0.49 ± 0.05 (n=3) (Q3N: Fig. 5A). The T4N mutant confers a significantly reduced fast inactivating component as the inactivation kinetics becomes dominated by the slower components (T4N: Fig. 5A). Inactivation of Kv4.2/Δ2-40 current conferred by T4N was best fitted by three exponential terms, with a fast inactivating component exhibiting time constant of 3.1 ± 0.3 ms and fractional amplitude of 0.22 ± 0.02 (n=5). Compared to the effects of Q3N, this represents a further significant reduction of the contribution of the DPP10a N-terminus to inactivation. The A5G mutant continues the trend of decreasing contribution of the fast inactivating phase, with the fast component from best three-exponential fits having a time constant of 3.4 ± 1.0 ms and fractional amplitude of 0.12 ± 0.05 (n=3) (A5G: Fig. 5A). Decreasing fractional amplitude of the fast inactivating component suggests the mutations destabilize the fast inactivated state; therefore, we examined the recovery from fast inactivation of Kv4.2/Δ2-40+Q3N channels. The results indicate that the Q3N substitution induced accelerated recovery from the fast phase of inactivation (Fig. 5B). A two-pulse protocol with a 25 ms-long initial inactivating pulse was used, and the time constants for recovery from inactivation at −100 mV were 44 ± 1.9 ms for wild-type DPP10a (n=5) and 34 ± 0.5 ms for Q3N ($p = 0.00724$; n=3).

The slowing of slow inactivation by the presence of DPP10a-conferred fast inactivation described earlier is also evident here. Q3N, which confers robust fast inactivation, mediates biphasic inactivation kinetics with a slower component with a time constant of 800 ± 85 ms and fractional amplitude of 0.36 ± 3.9 (n=3). Compared to Q3N, the T4N mutant induces inactivation kinetics with a significantly decreased fast component, and the slow phase of inactivation is notably faster. The intermediate (term1) and slow (term2) components of inactivation have time constants of 117 ± 17 ms and 360 ± 14 ms and fractional amplitudes of 0.14 ± 0.02 and 0.61 ± 0.02, respectively. The slower components of inactivation induced by A5G (terms 1 and 2) exhibit parameters similar to those induced by T4N (τ: term 1 = 136 ± 15 ms, term 2 = 367 ± 8.7 ms; fractional amplitude: term 1 = 0.17 ± 0.023, term 2 = 0.65 ± 0.045, n=3).

In addition to testing whether DPP10a-conferred inactivation is sensitive to individual conservative mutations within the NQTA sequence, we also generated DPP10a mutants with

scrambled NQTA sequences to further test if fast inactivation conferred by DPP10a is dependent on a specific sequence or simply the overall physico-chemical properties of the residues involved. As Figure 5C shows, the NQTA sequence is vital to the DPP10a-conferred fast inactivation, as scrambled sequences can either disrupt or enhance DPP10a-conferred fast inactivation. Replacing MNQTA with MANQT removes fast inactivation (Fig. 5C). The inactivation kinetics mediated by the MANQT mutant was best fitted with two exponential terms (tau: term1 = 75 ± 2.6 ms, term 2 = 235 ± 3.3 ms; fractional amplitude: term 1 = 0.17 ± 0.012, term 2 = 0.81 ± 0.01, n=3). These values are similar to those of the N2T mutant, which also disrupts DPP10a-mediated fast inactivation. However, when MNQTA is permutated to MQANT, DPP10a-conferred fast inactivation is accelerated and stabilized, with a time constant of 2.8 ± 0.2 ms (n=3). While its contribution to the overall current decay is not significantly increased (fractional amplitude = 0.51 ± 0.042, n=3), the recovery from this fast inactivation is significantly slowed (τ at −100 mV: 78 ± 4.3 ms, n=3, p = 0.000134) (Fig. 5D). These results indicate that scrambling the NQTA sequence alters the kinetics of DPP10a-conferred fast inactivation, with some eliminating it and others accelerating it. Overall, these results show that the evolutionarily-conserved N-terminal region of DPP10a includes a fast ID specifically constrained by the sequence of the first five amino acids.

Internal TEA Competes with MNQTA-conferred Fast Inactivation, and the Free MNQTA Peptide Acts as a Soluble Fast Channel Blocker

The finding that the MNQTA N-terminal sequence is a cytoplasmic inactivation-conferring domain of DPP10a and DPP6a suggests that it may act by a direct pore-blocking mechanism. To test this hypothesis, we employed inside-out patches to examine the effect of an open channel blocker (TEA) on Kv4.2/Δ2-40+DPP10a currents, as well as the soluble MNQTA peptide on Kv4.2/Δ2-40+DPP10a/ΔNQTA currents. Because patch excision is known to accelerate the kinetics of the slow inactivation in Kv4 channels,[27] we allowed the channel kinetics to stabilize after patch excision and before application of TEA or peptide. Interestingly, the rapid inactivating component for the Kv4.2/Δ2-40+DPP10a channels in inside-out patches accounts for 73 ± 1% of total decay and has a time constant of 3.5 ± 0.1 ms (n=4), similar to the 3.2 ± 0.5 ms (n=3) value observed in whole-oocyte currents (Fig. 3A & 6A).

If TEA and the DPP10a N-terminal ID compete for an internal site in the pore, a direct proportionality between the apparent current block and the slowing of MNQTA-conferred fast inactivation must occur.[20] Our results show that 10 mM internal TEA decreases peak current of Kv4.2/Δ2-40+DPP10a channels by 46 ± 2% (n=4) (Fig. 6A). The inactivation kinetics after the introduction of 10 mM internal TEA remains bi-exponential (Fig. 5A, fitted traces), with the fast component consisting of 71 ± 3% (n=5) of total current amplitude. However, the time constant of the fast component is slowed by internal TEA, increasing to 5.7 ± 0.3 ms (n=4). For clarity, the fast inactivating phases before and after TEA application, as determined by bi-exponential fitting, are superimposed to show the crossing-over of the currents before and after TEA addition (Fig. 6A). The slowing of the development of fast inactivation by TEA is also detectable by normalizing and superimposing the currents, and the effect is reversible upon washout (Fig. 6B). Next, we compared the fold-change in the fast time constant against the fold-change in the peak current at 5 and 10 mM TEA (Fig. 6C). There is a directly proportional relation between these changes, as the slope of the linear regression is ~1 and the corresponding intercept is 0, which is consistent with a direct competition between TEA binding in the pore and pore occlusion by the DPP10a N-terminal ID. Interestingly, like the DPP10a N-terminal ID, internal TEA also slows the inactivation kinetics of the slow phase (τ_S, 10 mM TEA: before = 19 ± 1 ms (n=4); after = 30 ± 1 ms, n=4)

To further test this hypothesis of a direct open channel block by the DPP10a ID, we asked whether the MNQTA peptide may act as a diffusible inactivation particle capable of occluding the pore of Kv4 channels.[15] The MNQTA peptide was chemically synthesized and applied to the cytoplasmic face of inside-out patches from tsA-201 cells co-expressing Kv4.2/Δ2-40 and DPP10a/ΔNQTA. Application of 300 μM MNQTA peptide suppressed 63% of the peak current (% remaining = 37 ± 2, n=3) (Fig. 7A); and this inhibition was quickly reversible upon washout (Fig. 7A & 7B). Blockage upon subsequent internal application of TEA confirmed the integrity of the channels in the inside-out patch (Fig. 7B). Although the MNQTA peptide suppressed the peak current, it did not produce the anticipated acceleration of inactivation; instead, the peptide slowed intrinsic inactivation (Fig. 7A). The time constant for the dominant inactivating component of the Kv4.2/Δ2-40+DPP10a/ΔNQTA, which had accelerated to 9.9 ± 0.4 ms (n=3) following patch excision, was slowed to 21.5 ± 1.2 ms (n=3) by application of the MNQTA peptide. Interestingly, the slowing of inactivation by MNQTA peptide resembles the slowing of slow phase of Kv4.2/Δ2-40+DPP10a inactivation by internal TEA or the tethered MNQTA ID. Overall, the results indicate that the 5-mer MNQTA peptide is able to block the Kv4.2 current in a manner analogous to TEA, a fast open-channel pore blocker.

DPP10a-conferred Fast Inactivation Is Insensitive to Elevated External K^+

Elevated external K^+ concentration does not affect the development of N-type inactivation in ShakerB Kv channels, but it accelerates the recovery from inactivation.[15, 21, 28] Since N-type inactivation in Shaker Kv channels also works by a pore-blocking mechanism, we examined the effect of elevated external K^+ concentration on DPP10a-mediated fast inactivation using a Kv4.2 channel lacking an N-terminal inactivation domain (Kv4.2/Δ2-40) as background construct. The slow inactivation of Kv4.2 channels in the absence of the endogenous N-terminal ID is accelerated by elevated external K^+ (Fig. 8A).[29] The time course for inactivation of Kv4.2/Δ2-40 channels is well described with two time constants, the values of which are decreased by the increase in external K^+ concentration (Fig. 8D). In addition to the acceleration of both phases of inactivation, the overall acceleration of inactivation by elevated $[K^+]_{ext}$ can be attributed to a significant increase in the fractional amplitude of the fast component (term 1) and a decrease in the slow component (term 2) (Fig. 8E).

Strikingly, like fast inactivation of ShakerB Kv channels, the time constant for fast inactivation induced by DPP10a is unaffected by 98 mM external K^+ (Fig. 8B). The DPP10a-induced fast inactivation accounts for the approximately half of the total decay, and the fast time constants from three exponential fits were 3.2 ± 1 ms and 3.2 ± 0.3 ms under 2 mM and 98 mM external K^+, respectively. This effect on fast inactivation contrasts with the striking acceleration of the residual slower phases of inactivation, leading to a decrease in the remaining current at the end of 1 sec depolarization (Fig. 8B). The results of tri-exponential fits indicate that the observation is due to the acceleration of the slow inactivation kinetics, since the time constants of exponential terms 2 is significantly decreased (Fig. 8D). The data also shows a marked increase in the fractional amplitude of exponential term 2 (Fig. 8E) with a concomitant decrease in the non-inactivating component (data not shown).

To show that the MNQTA sequence is responsible for the DPP10a-conferred, high-K^+-insensitive inactivation, DPP10a deletion mutant without residues NQTA was co-expressed with Kv4.2/Δ2-40. Accordingly, the entire time course of the Kv4.2/Δ2-40+DPP10a/ΔNQTA current at +50 mV shows significantly faster kinetics with 98 mM external K^+ (Fig. 8C). As summarized in Figures 8D and 8E, the time constants of the two phases decreased in value when external K^+ concentrations increased from 2 to 98 mM, while the fractional amplitudes remained unchanged. This result, along with the differential effects of

patch excision on distinct components of inactivation discussed previously, adds support to the likely role of the DPP10a N-terminal MNQTA sequence as the ID that confers fast inactivation..

Elevated External K^+ Concentration Accelerates Recovery from MNQTA-induced Fast Inactivation

In the Shaker N-type inactivation model, increasing external K^+ concentration results in an acceleration of recovery from inactivation at hyperpolarized potentials because (1) K^+ from the outside relieves the block by the inactivation peptide, and (2) unblocking by the peptide is necessary for recovery from inactivation.[16, 21] To determine whether Exon 1a-generated inactivation that also shares this property with ShakerB N-type inactivation, we investigated whether recovery from inactivation induced by the DPP10a N-terminal ID is accelerated by high external K^+ concentrations. Recovery from inactivation was measured by first briefly inactivating channels with a 25-ms depolarization to +50 mV, followed by a second 250-ms test pulse to +50 mV after an interpulse interval of variable duration at −100 mV. A pulse length of 25 ms was chosen because it is sufficiently long to allow completion of fast MNQTA-mediated fast inactivation (5 times the fast time constant of ~ 5 ms) without allowing excessive entry into slower inactivation. The double-pulse experiments show that Kv4.2/Δ2-40+DPP10a channels recover from MNQTA-mediated inactivation at a faster rate when external K^+ concentration is significantly increased from 2 mM to 98 mM (τ at −100 mV: 2 mM = 44 ± 2 ms, n=4; 98 mM = 25 ± 2 ms, n=3; $p = 1.85 \times 10^{-4}$) (Fig. 9A & 9B). In addition, the time course of the tail current matches the time course of recovery from inactivation, suggesting re-opening of inactivated channels prior to closing and recovery (Fig. 9C).[21] To verify that the acceleration of the recovery from inactivation is due to the MNQTA ID, we also determined the time course of recovery from inactivation for Kv4.2/Δ2-40+DPP10a/ΔNQTA with 2 and 98 mM external K^+ concentration (Fig. 9D). The duration of the inactivating pulse of the two-pulse protocol in this case was 1000 ms to allow maximum inactivation of these channels. The results showed that there is no acceleration of recovery at elevated $[K^+]_{ext}$, suggesting that the intact DPP10a N-terminus is required to observed acceleration of inactivation under high external K^+ concentration. Similar results were observed when ternary complex channels composed of Kv4.2, KChIP3a, and DPP10 subunits were substituted for binary complex channels (Supplementary Fig. S1). In summary, elevated external K^+ affected recovery from fast inactivation mediated by the MNQTA ID in a manner similar to Shaker N-type inactivation. This result, together with the results indicating that MNQTA acts as pore blocker that competes with internal TEA, provides compelling evidence for a mechanism of fast inactivation involving blockage of open Kv4.2 channels by the MNQTA ID of DPP10a.

DISCUSSION

We have examined the mechanism of the fast inactivation process conferred by DPP10a and DPP6a, two auxiliary subunits of Kv4 channels. This study shows that DPP6a is a paralog of DPP10a, DPP6a and DPP10a confer similar fast inactivation, and the highly-conserved N-terminal MNQTA motif is a novel ID underlying fast inactivation kinetics in a significant subclass of neuronal I_{SA} channels. This discovery of this N-terminal ID explains previously published observations showing: (1) Attenuation of accelerated fast inactivation by N-terminal tagging of DPP10a with a hemagglutinin epitope, (2) transfer of DPP10a-mediated fast inactivation from DPP10a to DPP6-S by N-terminal chimera construction, and (3) specific association of fast inactivation with the DPP10a N-terminal variant and not DPP10c or DPP10d.[7, 11] Furthermore, additional results indicate that interactions between the MNQTA motif and an internal site in the pore of Kv4 channels are critical in conferring fast inactivation by open-channel blockage.

MNQTA Confers Fast Kv4 Channel Inactivation with Pore-blocking Features

The experimental evidence presented here demonstrates that the MNQTA motif in DPP10a is responsible for introducing fast Kv4 inactivation. A molecular mechanism where the N-terminal MNQTA peptide rapidly binds and blocks the inner pore of Kv4 channels similar to N-type inactivation of Shaker-type channels provides the simplest explanation for our observations. The MNQTA sequence functions as a soluble inhibitory peptide that blocks the channel reversibly from the intracellular side of the membrane. The tethered MNQTA peptide mediates fast inactivation that competes with TEA for an internal pore blocking site (Fig. 10). Since TEA binds within an internal cavity of Kv channels and blocks the pore,[30–32] the DPP10a N-terminal ID may do the same to produce fast inactivation. Importantly, elevating external K^+ concentration accelerates recovery from MNQTA-induced fast inactivation, suggesting that the sequence may enter the open pore to block the conducting pathway.

Our finding that slow inactivation is impeded by the presence of intact MNQTA ID, internal TEA, and internally perfused MNQTA peptide also suggests that they are working by the same open-channel block mechanism. In Kv4 channels, slow inactivation is associated with closed-state inactivation (CSI). In CSI, Kv4 channels may inactivate directly from partially-activated closed states; and whenever the channels open ($C \rightarrow O$), they prefer to close ($O \rightarrow C$) to reach the absorbing closed-inactivated states ($C \rightarrow I_C$; Fig. 10).[1, 33, 34] Another important property of CSI in Kv4 channels is that it slows with stronger depolarizations of the membrane potential because voltage-dependent gating promotes opening and thereby decreases the probability of entering the inactivation-permissive pre-open closed state.[35] Similarly, internally-applied TEA rapidly blocks open channels, which stabilizes the open state. Since blocked channels cannot close, TEA effectively slows CSI of Kv4 channels. Both the intact MNQTA ID and free MNQTA peptide are likely to work by blocking the open channel, stabilizing the open state and thus slowing CSI.

We also provide evidence against modulations of P/C-type inactivation and CSI by the DPP10a MNQTA motif. In Kv4 channels, elevated external K^+ concentrations slow vestigial P/C-type inactivation by a “foot-in-the-door” mechanism directly and promote entry into CSI indirectly. [29, 36, 37] In contrast, the rate of fast Kv4.2 channel inactivation conferred by the DPP10a MNQTA ID is insensitive to elevated external K^+ concentrations (Fig. 8). Moreover, patch excision of Kv4.2/Δ2-40+DPP10a/ΔNQTA channels dramatically accelerates the slow inactivation process associated with CSI, but it does not affect the fast inactivation of Kv4.2/Δ2-40+DPP10a channels. Consistent with a distinct open-channel blocking mechanism of fast inactivation determined by the MNQTA ID, DPP10a consistently confers fast inactivation with identical kinetics (τ = ~4–6 ms) in spite of various manipulations that modify gating, including co-expression with KChIP3a or KChIP4a, and N-terminal deletion.[11] The similarity between the inactivation kinetics of Kv4.2+KChIP3a +DPP10a currents and I_{SA} from DPP10a-expressing cortical pyramidal neurons suggests that fast inactivation determined by MNQTA-induced pore blockage is present under native conditions.[11]

MNQTA, a Novel Sequence Evolutionarily Conserved for Fast Inactivation

We have demonstrated that the MNQTA sequence functions as an ID that blocks the channel pore, and the MNQTA sequence specifically produces the kinetic properties of DPP10a-conferred fast inactivation. Most of the individual conservative substitutions in the tethered MNQTA sequence cause dramatic disruptions of fast inactivation, suggesting a rationale for evolutionary preservation. Furthermore, scrambling of the NQTA sequence in the intact DPP10a protein also produces severe changes in the inactivation kinetics. Whereas the MANQT mutant fails to mediating fast inactivation, the MQANT mutant induces an

even faster inactivation. Therefore, fast inactivation induced by DPP10a and DPP6a depends on interactions specifically constrained by the MNQTA sequence at the N-terminus of these ancillary subunits.

The free MNQTA peptide blocks the Kv4 channel but does not induce time-dependent fast inactivation as observed for other free K^+ channel ID peptides.[16], [19], [38] This suggests that studies using free MNQTA peptide, unconstrained by the rest of DPP10a, may not truly mimic fast inactivation induced by DPP10a or DPP6a. Similar to our result, a 4-mer peptide corresponding to the first four amino acids of the rat Kvβ1 N-type ID also produces fast instantaneous blockage of Kv1.4 channels without inducing a time-dependent blockage.[39] In another similar case, the KIFMK peptide corresponding to the ID of voltage-gated Na^+ channels induces open channel blockage that does not mimic native fast inactivation.[40] Therefore, in contrast to the tethered IDs or long ID peptide, small free peptides most likely act like TEA as fast pore blockers and are not likely to produce mechanistic information relevant to the intact tethered ID.

Our NQTA point mutations, in combination with sequence scrambling mutations, provided more insights into the nature of the MNQTA motif. The DPP10a N2T mutant cannot induce fast inactivation, suggesting a critical role of N2 residue in fast inactivation. Interestingly, the MANQT mutant, with a non-conservative, polar-to-hydrophobic mutation the second position also abolishes fast inactivation. The Q3N mutant shows that fast inactivation might be more tolerant to alterations at the third position. Indeed, when alanine is located at position 3 in the MQANT scrambled mutant, fast inactivation became faster. In addition, the Q3N and MQANT mutants show that residues in the N-terminal ID can also affect the kinetics of recovery from inactivation. A significant difference in the kinetics of recovery from inactivation was also detected between Kv4.2+KChIP3a channel co-expressed with either DPP10a or DPP6a (Fig. 2D). We propose that the difference may be due to specific interactions formed during pore block that stabilize the blocked structure.

Interestingly, the novel MNQTA motif differs significantly from the ID sequence generally described for Shaker N-type, “ball-and-chain” inactivation; in sharp contrast to the ShakerB ID, the MNQTA sequence is not significantly hydrophobic. Since such hydrophobic residues have been shown to be crucial determinants of the ShakerB ID binding affinity,[41], [42] it is probable that the interactions between the MNQTA sequence and the channel may differ from those in the ShakerB channel, thereby affecting association and dissociation rate constants. We can estimate the peptide unbinding rate constant (k_{ub}) by assuming a two-state model where 1) channels are either open or blocked by MNQTA and 2) the amplitude of the non-MNQTA-induced component represents a good estimate of the unblocked level of the current after MNQTA ID block. According to this model, $k_{ub} = I_s/\tau_{fast}$, (where I_s is the fractional amplitude of the unblocked current and τ_{fast} is the time constant of the fast component). The results show that the k_{ub} values for Kv4.2+KChIP3a+DPP10a (37 ± 2 s^{-1}, n=6), Kv4.2+KChIP3a+DPP6a (50 ± 3 s^{-1}, n=4), and Kv4.2/Δ2-40+DPP10a (95 ± 16 s^{-1}, n=4) are all significantly larger than those of the peptides corresponding to the IDs of ShB (~14 s^{-1}) and Kv3.4 (~11 s^{-1}).[42] For the Kv4.2 N-terminal ID, Gebauer et al. (2004) reported an unbinding rate constant of the order of 9–19 s^{-1}, which are comparable to those of the ShakerB and Kv3.4 IDs. Although the ShakerB, Kv3.4 and Kv4.2 IDs share weak similarity, their binding may depend mainly on hydrophobic interactions.[19], [41] Indeed, the interacting residues between the Shaker Kv channel ID and its receptor have been identified in the proximal N-terminus and in S6,[39] and Gebauer et al. (2004) showed by using mutant cycle analysis that a putative interaction exists between the hydrophobic residues Ala3 and Val406 of Kv4.2.[19] Interestingly, in contrast with the importance of residue 3 in the studies by Zhou et al. (2001) and Gebauer et al. (2004), our Q3N mutant shows the least amount of disruption to MNQTA-conferred inactivation among the mutations examined. Further work

will be necessary to determine how the more polar character of the MNQTA ID influences its ability to bind to a putative pore site in Kv4.2 channels.

Physiological Implications in Native I_{SA} Channels

The molecular basis of DPP10a- and DPP6a-mediated fast inactivation is particularly relevant for understanding I_{SA} inactivation in neurons in which these isoforms are expressed. In adult rats, DPP10a transcript is selectively expressed in cortical pyramidal neurons of layers 2/3 and 5, and I_{SA} from cortical neurons can be recapitulated by transient currents generated upon heterologous coexpression of Kv4.2, KChIP3a, and DPP10a.[11] According to a recent report, the DPP6a transcript is expressed in the hippocampus, intermediary layer of the superior colliculus, and cerebellar granule neurons of p30 mouse brain, and coexpression of DPP6a (DPP6-E) and DPP6-S at a 1:2 ratio is needed to reproduce the inactivation kinetics of I_{SA} from cerebellar granule neurons.[10] Our own determination of the DPP6a mRNA expression pattern in p12 rat brain provided a slightly different result, with detection of DPP6a transcripts in cerebellar granule neurons and neurons of the superior colliculus, red nucleus, piriform cortex, thalamus, magnocellular preoptic nucleus, central medial nucleus, paracentral nucleus thalamus, and mediodorsal/medial nucleus thalamus, brachium of the inferior colliculus, and pontine grey.[22] We do not know whether differences in species, age, or technique (*in situ* hybridization with digoxigenin- or radio-labelled probes) accounts for the differences. Nevertheless, these expression patterns indicate that DPP6a and DPP10a are putative molecular determinants of fast I_{SA} inactivation in several neuronal populations in the adult brain. Future experiments will be necessary to determine the DPP10a and DPP6a protein levels in their respective neuronal types and directly demonstrate their role in shaping the inactivation of neuronal I_{SA}.

The results of Kv4 ternary complex studies imply that DPP10a and DPP6a confer fast inactivation of I_{SA} by a pore blocking mechanism in neurons expressing these specific isoforms. Since Kv4-based channels dampen neuronal excitability, drugs that oppose Kv4 inactivation would be useful for treating pathological hyperexcitability resulting from neurological disorders such as epilepsy. Recently, small molecular inhibitors have been discovered that can “disinactivate” N-type inactivation of Kv1.4 and Kv1.1+Kvβ1 channels, increasing time constant of inactivation.[43, 44] Future development of a disinactivator specific for fast inactivation mediated by DPP10a or DPP6a may have potentially therapeutic applications for specific neuronal populations where they are expressed. Second, DPP10a and DPP6a may play important roles in firing properties. Saito & Isa (2000) showed a correlation between I_{SA} inactivation kinetics and firing properties of neurons from the superior colliculus, where DPP6a is strongly expressed.[10, 45, 46] Altering the expression levels of specific DPLP isoforms in these neurons, using strategies such as RNA interference, should allow us to examine the influence of modulating inactivation kinetics on somatodendritic excitability. These and other pharmacological and molecular approaches to target DPP6 and DPP10 modulation of I_{SA} may prove useful, as genetic variations in these auxiliary subunits are increasingly linked to neurological disorders such as amyotrophic lateral sclerosis, autism spectrum disorder, progressive spinal muscular atrophy.[47–50]

MATERIALS & METHODS

Molecular Biology

Plasmids containing DPP10a and DPP6-S cDNAs were described previously.[7] DPP6 Exon 1a was amplified from whole brain cDNA of p21 Sprague-Dawley rat and used to swap out DPP6 Exon 1s by subcloning, resulting in full-length DPP6a cDNA. Kv4.2/Δ2-40, DPP10a/Δ2-20, and DPP10a/ΔNQTA coding sequences were amplified by PCR using primers

designed with nested restriction enzyme sites, and the cDNAs were maintained in pBluescript-based vectors. N2T, Q3N, and A5G constructs were generated by QuikChange Site Directed Mutagenesis (Stratagene) using appropriate primers, and T4N, MQANT, and MANQT constructs were generated by first amplifying an insert containing the mutations (located right in the overlapped segment) by overlap extension and then subcloning the fragment into DPP10a construct. For hetereologous expression in tsA-201 cells, Kv4.2/Δ2-40, DPP10a, DPP10a/ΔNQTA, and DPP10a/Δ2-20 cDNAs were maintained in pCMV-N/C (Clonetech). All sequences were checked and verified by automated sequencing (DNA sequencing core facility at Baylor College of Medicine, Houston, TX).

Heterologous Expression of Kv4 Constructs

Experiments on *Xenopus laevis* frogs were performed in accordance with a protocol approved by the Institutional Animal Care and Use Committees (IACUC) of Baylor College of Medicine. For oocyte harvest, frogs were anaesthetized with 0.1% ethyl 3-aminobenzoate methanesulfonate (Tricane) absorbed through the skin. Stage V–VI oocytes were surgically harvested through a small incision in the lower abdomen and defolliculated by collagenase I treatment. The incision was sutured immediately after oocyte harvest. Each frog is used for 2–5 surgeries before euthanasia by decapitation and double pithing under anaesthesia. A Nanoinjector (Drummond, Broomall, PA) was used to inject oocytes with Kv4.2 cRNA (typically 2–4 ng/oocyte) with or without auxiliary subunit cRNAs. Before testing, injected oocytes were incubated at 18°C for 1–3 days in standard ND96 solution (in mM: 96 NaCl, 2 KCl, 1.8 $CaCl_2$, 1 $MgCl_2$, and 5 HEPES, pH 7.4 adjusted with NaOH) supplemented with 5 mM Na-pyruvate and 5 μg/ml gentamycin. For studies in mammalian cells, tsA-201 cells (a gift from Dr. Richard Horn, Thomas Jefferson University) were transfected using the calcium-phosphate method.[51] Co-transfection of a plasmid containing the CD8 gene allows the identification of individual transfected cells by labelling them with beads bearing anti-CD8 antibody (Dynal).[52]

Electrophysiology

Whole-cell currents from injected oocytes were elicited using the two-electrode voltage clamp technique. The microelectrodes, with <1 MΩ tip resistance, were filled with 3 M KCl solutions. The voltage-clamp amplifier (Oocyte Clamp OC-725, Warner Instruments, Hamden, CT) operated under the control of either the pClamp6 (Axon instruments, Foster City, CA) or WinWCP software (John Dempster, University of Strathclyde, Glasgow, UK). The data were digitized and low-pass filtered (Frequency Devices, Haverhill, MA) at various frequencies depending on the sampling rate. The capacitative transients were subtracted off-line by scaling up transients at voltages without ionic currents (at either −70 or −90 mV) and subtracting them from total currents. Only recordings with offsets <2 mV were analysed, and the average leak current was <0.2 μA and subtracted off-line, assuming Ohmic leak.

Macroscopic K^+ currents from tsA-201 cells, a transformed HEK293 cell line,[53] were measured using the cell-attached and inside-out patch clamp configuration with the following solutions: bath solution (internal; in mM) 105 KF, 35 KCl, 10 EGTA, and 10 HEPES, pH 7.41 with KOH, and pipette solution (external; in mM) 150 NaCl, 2 KCl, 1.5 $CaCl_2$, 1 $MgCl_2$, 10 HEPES, pH 7.38. KCl was replaced by TEA-Cl in internal solutions containing TEA. Currents were elicited by 400 ms step depolarizations to +42 mV from a holding potential of −108 mV every 10 seconds. Currents were filtered at 2 KHz and sampled at 10 KHz. The calculated liquid junction potential was subtracted off-line. Recordings of both oocyte and tsA-201 membrane currents were performed at room temperature (22–25°C).

The MNQTA peptide with C-terminal amide was synthesized and HPLC purified (Protein Chemistry Core Laboratory of Baylor College of Medicine). After establishing a stable current baseline, the MNQTA peptide was added to the bath until the current reached a new stable level. Then, washout was implemented to evaluate recovery.

Data Analysis

Digitized voltage-clamp data from oocyte recordings were analysed with Clampfit (Axon Instruments), WinWCP (John Dempster, University of Strathclyde, Glasgow, UK), and Origin software (OriginLab Corp., Northampton, MA). Analyses and graphical displays of tsA-201 data were produced with pClamp (version 10.0; Molecular Devices) and Origin (version 7.5; OriginLab) software. Peak conductance (Gp) was calculated as

$$Gp=Ip/(Vc - Vrev),$$

where Ip is the peak current, Vc is the command voltage, and Vrev is the reversal potential (−90 mV in ND96). Peak conductance-voltage (Gp-V) curves were described using fourth-powered Boltzmann function:

$$Gp/Gpmax=1/(1+\exp(Vm - V_a)/k))^4,$$

where Gp/Gpmax is the fraction of maximal conductance, Vm is the membrane potential, V_a is the potential for half-maximal activation of one subunit, and k is the slope factor. The mid-point voltages of the Gp-V curve (V0.5) were calculated using the following equation:

$$V_{0.5}=(V_a+(k \times 1.665))$$

Steady-state inactivation is also using a single Boltzmann function. The time courses of recovery from inactivation were measured using a two-pulse protocol. Briefly, two pulses to +50 mV (inactivating pulse and test pulse) were separated by a variable recovery interval at −100 mV to determine the time required for channel recovery. The results for recovery from inactivation were fitted with either a single or double exponential function, depending on the fit. Data are presented as mean ± standard error of the mean (SEM). Pairs of data were compared for statistical significance using Student's two-tailed (independent) *t* test. Significance is determined when $p < 0.05$.

Supplementary Material

Refer to Web version on PubMed Central for supplementary material.

Acknowledgments

This work was supported by National Institute of Health grant P01 NS37444 (to HHJ and PJP), NIH training grant T32 AA07463 (to KD) and National Institute of Health grant R01 NS032337 (to MC).

Abbreviations & Acronyms

DPP6	dipeptidyl peptidase 6
DPP10	dipeptidyl peptidase 10

DPLP	dipeptidyl peptidase-like protein
KChIP	Kv channel-interacting protein
I_{SA}	subthreshold A-type K+ current
TEA	tetraethylammonium
AP	action potential
ID	inactivation domain
CSI	closed-state inactivation
RACE	rapid amplification of 5′ complementary DNA ends
EST	expressed sequence tag

References

1. Jerng HH, Pfaffinger PJ, Covarrubias M. Molecular physiology and modulation of somatodendritic A-type potassium channels. Mol Cell Neurosci. 2004; 27:343–369. [PubMed: 15555915]
2. Birnbaum SG, Varga AW, Yuan LL, Anderson AE, Sweatt JD, Schrader LA. Structure and function of Kv4-family transient potassium channels. Physiol Rev. 2004; 84:803–833. [PubMed: 15269337]
3. Covarrubias M, Bhattacharji A, De Santiago-Castillo JA, Dougherty K, Kaulin YA, Na-Phuket TR, Wang G. The neuronal Kv4 channel complex. Neurochem Res. 2008; 33:1558–1567. [PubMed: 18357523]
4. Maffie J, Rudy B. Weighing the evidence for a ternary protein complex mediating A-type K+ currents in neurons. J Physiol. 2008; 586:5609–5623. [PubMed: 18845608]
5. An WF, Bowlby MR, Betty M, Cao J, Ling HP, Mendoza G, Hinson JW, Mattsson KI, Strassle BW, Trimmer JS, Rhodes KJ. Modulation of A-type potassium channels by a family of calcium sensors. Nature. 2000; 403:553–556. [PubMed: 10676964]
6. Nadal MS, Ozaita A, Amarillo Y, Vega-Saenz de Miera E, Ma Y, Mo W, Goldberg EM, Misumi Y, Ikehara Y, Neubert TA, Rudy B. The CD26-related dipeptidyl aminopeptidase-like protein DPPX is a critical component of neuronal A-type K+ channels. Neuron. 2003; 37:449–461. [PubMed: 12575952]
7. Jerng HH, Qian Y, Pfaffinger PJ. Modulation of Kv4.2 channel expression and gating by dipeptidyl peptidase 10 (DPP10). Biophys J. 2004; 87:2380–2396. [PubMed: 15454437]
8. Dougherty K, Covarrubias M. A dipeptidyl aminopeptidase-like protein remodels gating charge dynamics in Kv4.2 channels. J Gen Physiol. 2006; 128:745–753. [PubMed: 17130523]
9. Jerng HH, Kunjilwar K, Pfaffinger PJ. Multiprotein assembly of Kv4.2, KChIP3 and DPP10 produces ternary channel complexes with ISA-like properties. J Physiol. 2005; 568:767–788. [PubMed: 16123112]
10. Maffie J, Blenkinsop T, Rudy B. A novel DPP6 isoform (DPP6-E) can account for differences between neuronal and reconstituted A-type K(+) channels. Neurosci Lett. 2009; 449:189–194. [PubMed: 19007856]
11. Jerng HH, Lauver AD, Pfaffinger PJ. DPP10 splice variants are localized in distinct neuronal populations and act to differentially regulate the inactivation properties of Kv4-based ion channels. Mol Cell Neurosci. 2007; 35:604–624. [PubMed: 17475505]
12. Pruunsild P, Timmusk T. Structure, alternative splicing, and expression of the human and mouse KCNIP gene family. Genomics. 2005; 86:581–593. [PubMed: 16112838]
13. Nadal MS, Amarillo Y, Vega-Saenz de Miera E, Rudy B. Differential characterization of three alternative spliced isoforms of DPPX. Brain Res. 2006; 1094:1–12. [PubMed: 16764835]
14. Takimoto K, Hayashi Y, Ren X, Yoshimura N. Species and tissue differences in the expression of DPPY splicing variants. Biochem Biophys Res Commun. 2006; 348:1094–1100. [PubMed: 16899223]

15. Hoshi T, Zagotta WN, Aldrich RW. Biophysical and molecular mechanisms of Shaker potassium channel inactivation. Science. 1990; 250:533–538. [PubMed: 2122519]
16. Ruppersberg JP, Frank R, Pongs O, Stocker M. Cloned neuronal IK(A) channels reopen during recovery from inactivation. Nature. 1991; 353:657–660. [PubMed: 1922383]
17. Heinemann SH, Rettig J, Graack HR, Pongs O. Functional characterization of Kv channel beta-subunits from rat brain. J Physiol. 1996; 493 (Pt 3):625–633. [PubMed: 8799886]
18. Covarrubias M, Wei A, Salkoff L, Vyas TB. Elimination of rapid potassium channel inactivation by phosphorylation of the inactivation gate. Neuron. 1994; 13:1403–1412. [PubMed: 7993631]
19. Gebauer M, Isbrandt D, Sauter K, Callsen B, Nolting A, Pongs O, Bahring R. N-type inactivation features of Kv4.2 channel gating. Biophys J. 2004; 86:210–223. [PubMed: 14695263]
20. Choi KL, Aldrich RW, Yellen G. Tetraethylammonium blockade distinguishes two inactivation mechanisms in voltage-activated K+ channels. Proc Natl Acad Sci U S A. 1991; 88:5092–5095. [PubMed: 2052588]
21. Demo SD, Yellen G. The inactivation gate of the Shaker K+ channel behaves like an open-channel blocker. Neuron. 1991; 7:743–753. [PubMed: 1742023]
22. Jerng HH, Dougherty K, Covarrubias M, Pfaffinger PJ. Does DPP10a-mediated Fast Inactivation Involve An N-type-like Mechanism? Biophys J. 2008; 94:522.
23. Hough RB, Lengeling A, Bedian V, Lo C, Bucan M. Rump white inversion in the mouse disrupts dipeptidyl aminopeptidase-like protein 6 and causes dysregulation of Kit expression. Proc Natl Acad Sci U S A. 1998; 95:13800–13805. [PubMed: 9811881]
24. Wang H, Yan Y, Liu Q, Huang Y, Shen Y, Chen L, Chen Y, Yang Q, Hao Q, Wang K, Chai J. Structural basis for modulation of Kv4 K+ channels by auxiliary KChIP subunits. Nat Neurosci. 2007; 10:32–39. [PubMed: 17187064]
25. Dougherty K, Tu L, Deutsch C, Covarrubias M. The dipeptidyl-aminopeptidase-like protein 6 is an integral voltage sensor-interacting beta-subunit of neuronal K(V)4.2 channels. Channels (Austin). 2009; 3:122–128. [PubMed: 19372736]
26. Taylor WR. The classification of amino acid conservation. J Theor Biol. 1986; 119:205–218. [PubMed: 3461222]
27. Beck EJ, Covarrubias M. Kv4 channels exhibit modulation of closed-state inactivation in inside-out patches. Biophys J. 2001; 81:867–883. [PubMed: 11463631]
28. Tseng GN, Tseng-Crank J. Differential effects of elevating [K]o on three transient outward potassium channels. Dependence on channel inactivation mechanisms. Circ Res. 1992; 71:657–672. [PubMed: 1499110]
29. Kaulin YA, De Santiago-Castillo JA, Rocha CA, Covarrubias M. Mechanism of the modulation of Kv4:KChIP-1 channels by external K+ Biophys J. 2008; 94:1241–1251. [PubMed: 17951301]
30. Lenaeus MJ, Vamvouka M, Focia PJ, Gross A. Structural basis of TEA blockade in a model potassium channel. Nat Struct Mol Biol. 2005; 12:454–459. [PubMed: 15852022]
31. Faraldo-Gomez JD, Kutluay E, Jogini V, Zhao Y, Heginbotham L, Roux B. Mechanism of intracellular block of the KcsA K+ channel by tetrabutylammonium: insights from X-ray crystallography, electrophysiology and replica-exchange molecular dynamics simulations. J Mol Biol. 2007; 365:649–662. [PubMed: 17070844]
32. Yohannan S, Hu Y, Zhou Y. Crystallographic study of the tetrabutylammonium block to the KcsA K+ channel. J Mol Biol. 2007; 366:806–814. [PubMed: 17196615]
33. Jerng HH, Shahidullah M, Covarrubias M. Inactivation gating of Kv4 potassium channels: molecular interactions involving the inner vestibule of the pore. J Gen Physiol. 1999; 113:641–660. [PubMed: 10228180]
34. Bahring R, Boland LM, Varghese A, Gebauer M, Pongs O. Kinetic analysis of open- and closed-state inactivation transitions in human Kv4.2 A-type potassium channels. J Physiol. 2001; 535:65–81. [PubMed: 11507158]
35. Amarillo Y, De Santiago-Castillo JA, Dougherty K, Maffie J, Kwon E, Covarrubias M, Rudy B. Ternary Kv4.2 channels recapitulate voltage-dependent inactivation kinetics of A-type K+ channels in cerebellar granule neurons. J Physiol. 2008; 586:2093–2106. [PubMed: 18276729]

36. Lopez-Barneo J, Hoshi T, Heinemann SH, Aldrich RW. Effects of external cations and mutations in the pore region on C-type inactivation of Shaker potassium channels. Receptors Channels. 1993; 1:61–71. [PubMed: 8081712]
37. Jerng HH, Gilly WF. Inactivation and pharmacological properties of sqKv1A homotetramers in Xenopus oocytes cannot account for behavior of the squid “delayed rectifier” K(+) conductance. Biophys J. 2002; 82:3022–3036. [PubMed: 12023225]
38. Wallner M, Meera P, Toro L. Molecular basis of fast inactivation in voltage and Ca2+-activated K + channels: a transmembrane beta-subunit homolog. Proc Natl Acad Sci U S A. 1999; 96:4137–4142. [PubMed: 10097176]
39. Zhou M, Morais-Cabral JH, Mann S, MacKinnon R. Potassium channel receptor site for the inactivation gate and quaternary amine inhibitors. Nature. 2001; 411:657–661. [PubMed: 11395760]
40. Tang L, Kallen RG, Horn R. Role of an S4–S5 linker in sodium channel inactivation probed by mutagenesis and a peptide blocker. J Gen Physiol. 1996; 108:89–104. [PubMed: 8854339]
41. Murrell-Lagnado RD, Aldrich RW. Energetics of Shaker K channels block by inactivation peptides. J Gen Physiol. 1993; 102:977–1003. [PubMed: 8133246]
42. Murrell-Lagnado RD, Aldrich RW. Interactions of amino terminal domains of Shaker K channels with a pore blocking site studied with synthetic peptides. J Gen Physiol. 1993; 102:949–975. [PubMed: 8133245]
43. Zhang ZH, Rhodes KJ, Childers WE, Argentieri TM, Wang Q. Disinactivation of N-type inactivation of voltage-gated K channels by an erbstatin analogue. J Biol Chem. 2004; 279:29226–29230. [PubMed: 15136567]
44. Lu Q, Peevey J, Jow F, Monaghan MM, Mendoza G, Zhang H, Wu J, Kim CY, Bicksler J, Greenblatt L, Lin SS, Childers W, Bowlby MR. Disruption of Kv1.1 N-type inactivation by novel small molecule inhibitors (disinactivators). Bioorg Med Chem. 2008; 16:3067–3075. [PubMed: 18226531]
45. Jerng HH, Pfaffinger PJ. Tuning of native A-current properties by expression of auxiliary subunit alternative transcripts. Soc Neurosci Abstr. 2008; 34:234.216.
46. Saito Y, Isa T. Voltage-gated transient outward currents in neurons with different firing patterns in rat superior colliculus. J Physiol. 2000; 528(Pt 1):91–105. [PubMed: 11018108]
47. Cronin S, Berger S, Ding J, Schymick JC, Washecka N, Hernandez DG, Greenway MJ, Bradley DG, Traynor BJ, Hardiman O. A genome-wide association study of sporadic ALS in a homogenous Irish population. Hum Mol Genet. 2008; 17:768–774. [PubMed: 18057069]
48. van Es MA, van Vught PW, Blauw HM, Franke L, Saris CG, Van den Bosch L, de Jong SW, de Jong V, Baas F, van’t Slot R, Lemmens R, Schelhaas HJ, Birve A, Sleegers K, Van Broeckhoven C, Schymick JC, Traynor BJ, Wokke JH, Wijmenga C, Robberecht W, Andersen PM, Veldink JH, Ophoff RA, van den Berg LH. Genetic variation in DPP6 is associated with susceptibility to amyotrophic lateral sclerosis. Nat Genet. 2008; 40:29–31. [PubMed: 18084291]
49. Marshall CR, Noor A, Vincent JB, Lionel AC, Feuk L, Skaug J, Shago M, Moessner R, Pinto D, Ren Y, Thiruvahindrapduram B, Fiebig A, Schreiber S, Friedman J, Ketelaars CE, Vos YJ, Ficicioglu C, Kirkpatrick S, Nicolson R, Sloman L, Summers A, Gibbons CA, Teebi A, Chitayat D, Weksberg R, Thompson A, Vardy C, Crosbie V, Luscombe S, Baatjes R, Zwaigenbaum L, Roberts W, Fernandez B, Szatmari P, Scherer SW. Structural variation of chromosomes in autism spectrum disorder. Am J Hum Genet. 2008; 82:477–488. [PubMed: 18252227]
50. van Es MA, van Vught PW, van Kempen G, Blauw HM, Veldink JH, van den Berg LH. Dpp6 is associated with susceptibility to progressive spinal muscular atrophy. Neurology. 2009; 72:1184–1185. [PubMed: 19332697]
51. O’Leary ME, Horn R. Internal block of human heart sodium channels by symmetrical tetra-alkylammoniums. J Gen Physiol. 1994; 104:507–522. [PubMed: 7807059]
52. Jurman ME, Boland LM, Liu Y, Yellen G. Visual identification of individual transfected cells for electrophysiology using antibody-coated beads. Biotechniques. 1994; 17:876–881. [PubMed: 7840967]
53. Chahine M, Bennett PB, George AL Jr, Horn R. Functional expression and properties of the human skeletal muscle sodium channel. Pflugers Arch. 1994; 427:136–142. [PubMed: 8058462]

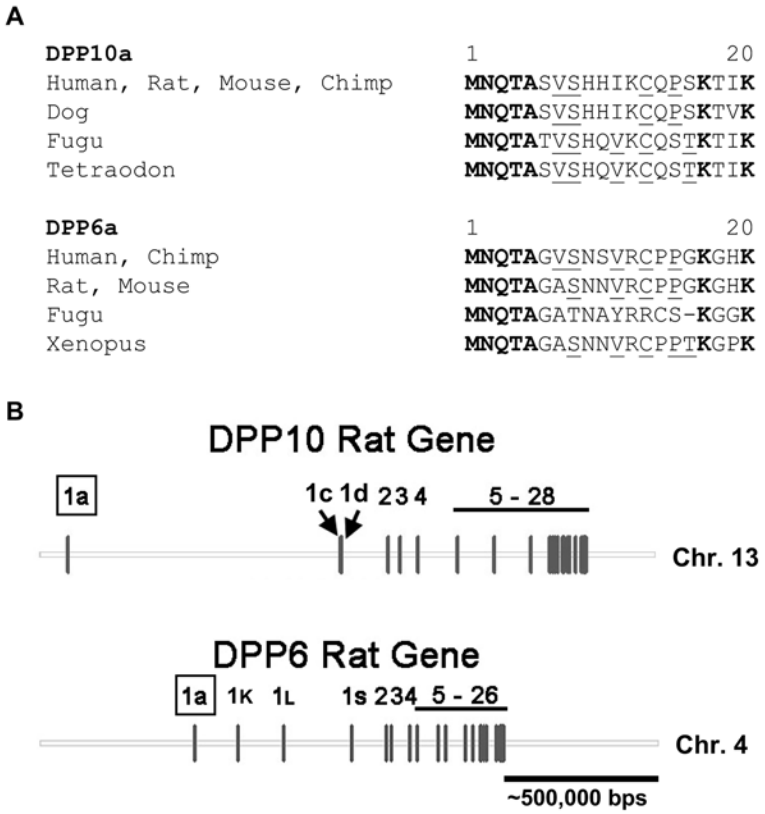

Figure 1. The Most Upstream of the Alternatively Spliced First Exons of DPP10a and DPP6a (Exon 1a) Encode Highly Similar Amino Acid Sequences

(A) Alignment of amino acids sequences encoded by Exon 1a of DPP10 and DPP6 from various species. Sequences were obtained by mining cDNA and genomic databases. Identical residues between DPP10a and DPP6a are shown in bold; consensus residues, underlined. Notice the identity between residues 1-5 (MNQTA) of these DPLP variants. (B) Genomic organization of rat DPP10 and DPP6 genes, including Exon 1's of known splice variants (DPP10: DPP10a, DPP10c, DPP10d; DPP6: DPP6a, DPP6-K, DPP6-L, DPP6-S). DPP10 rat gene is located on chromosome 13; DPP6, chromosome 4.

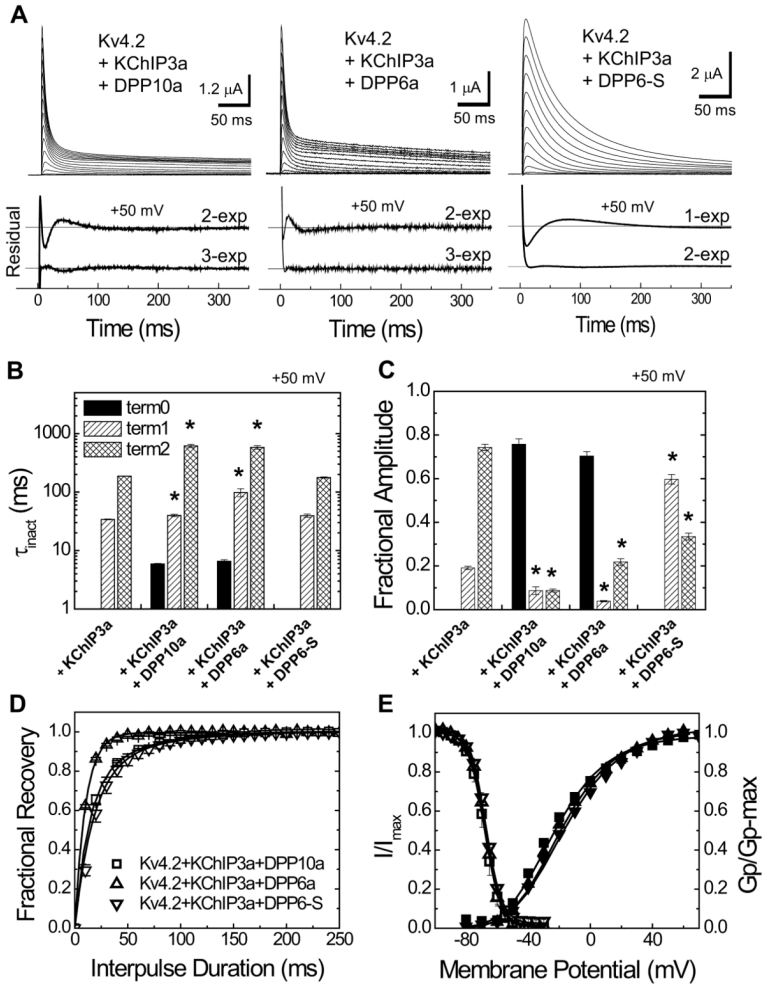

Figure 2. DPP10a and DPP6a Introduce a Similar Rapid Phase of Inactivation in Kv4.2+KChIP3a Channels

(A) DPP6a produces kinetic effects similar to those of DPP10a and very different from those of DPP6-S. Families of current traces were elicited by 10-mV step depolarizations of 1- or 5-sec duration from −100 mV to +60 mV, starting from a holding potential of −100 mV. Only the first 350 ms are shown. Inactivation kinetics at +50 mV were measured using multi-exponential fits, and based on the residuals (actual current traces minus fitted traces) Kv4.2+KChIP3a plus DPP10a or DPP6a requires three time constants to properly describe the decay (τ0, τ1, and τ2). However, the inactivation of Kv4.2+KChIP3a+DPP6-S channel is well-described by two time constants. Based on similarity of time constant values to currents modified by a-variants, the time constants were named τ1 and τ2. (B) The time course of inactivation at +50 mV. Notice the match between the fast time constants of Kv4.2+KChIP3a+DPP10a and Kv4.2+KChIP3a+DPP6a. (C) The fractional amplitudes of the inactivating components at +50 mV. The majority of the current undergoes fast inactivation in the presence of the intact DPP10a and DPP6a N-terminal domains. (D) Recovery from inactivation of Kv4.2+KChIP3a coexpressed with DPP6-S, DPP6a, and DPP10a at −100 mV. The standard two-pulse protocol was used, with a 1-sec long prepulse to +50 mV. (E) The peak conductance-voltage (Gp-V) relationships and steady-state inactivation curves for the channel complexes under study. Gp-V is best fit with a 4th-powered Boltzmann. Steady-state inactivation was fit with a single Boltzmann function. The symbols used are the same as in Fig. 2D, with I/I_{max} and Gp/Gp-max data points represented

by open and closed symbols, respectively. The Gp-V and steady-state inactivation curves are quite similar, despite differing inactivation kinetics. Asterisks indicate statistical significance with $p < 0.05$ when compared to corresponding control values.

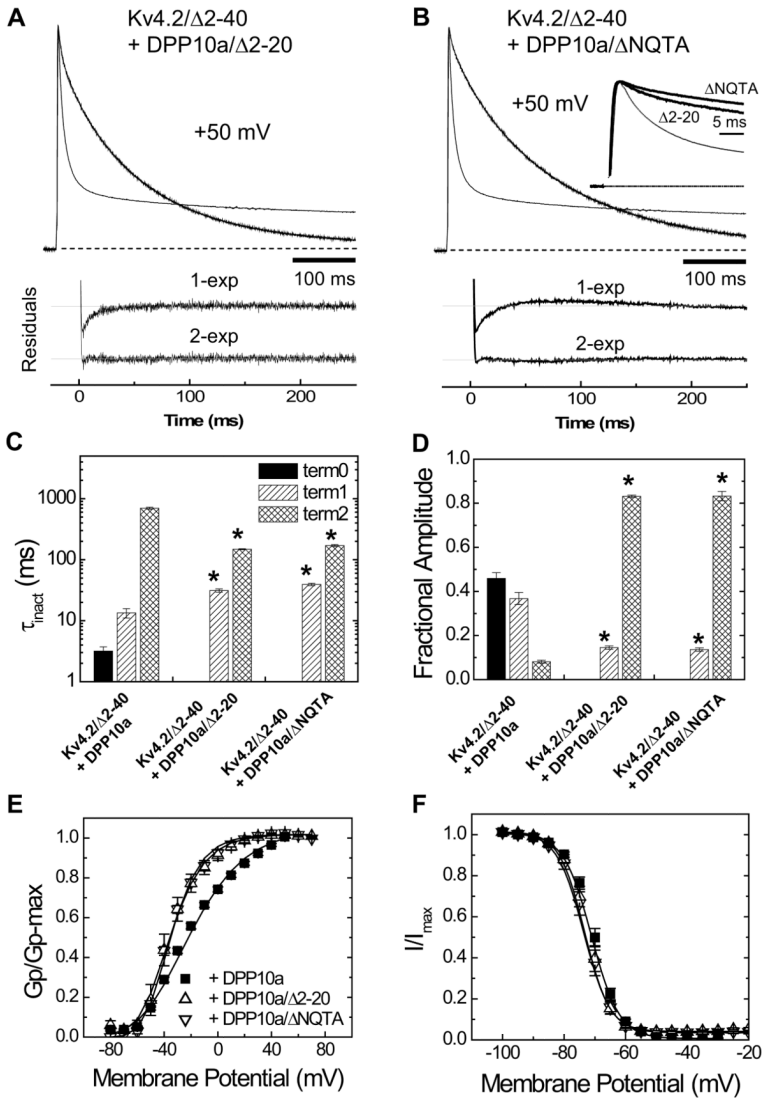

Figure 3. Deletion of DPP10a AA2-5 (NQTA) Is Sufficient to Eliminate DPP10a-mediated Fast Component of Inactivation

(A, B) Representative normalized current traces at +50 mV for Kv4.2/Δ2-40 coexpressed with DPP10a/Δ2-20 (A) and DPP10a/ΔNQTA (B). Traces were overlapped with normalized Kv4.2/Δ2-40+DPP10a trace (thin lines) to show kinetic differences. Rapid inactivation by DPP10a is eliminated by these N-terminal deletions. In panel B inset, traces are shown in smaller time scale to show similar activation kinetics. (C) Time constants of inactivating components at +50 mV for the channels under study. (D) Fractional amplitudes for inactivating components at +50 mV. (E) Normalized peak conductance-voltage (Gp-V) relationships. The Gp-V curves were analyzed as described in Materials and Methods. Deletions of MNQTA and residues 2-20 similarly produce ~ 15 mV leftward shift in the $V_{0.5}$ value. (F) Measurements of steady-state inactivation at indicated membrane potentials. According to Boltzmann fit, no significant changes in midpoint or slope were produced by the deletions. Asterisks indicate statistical significance with $p < 0.05$ when compared to corresponding control values.

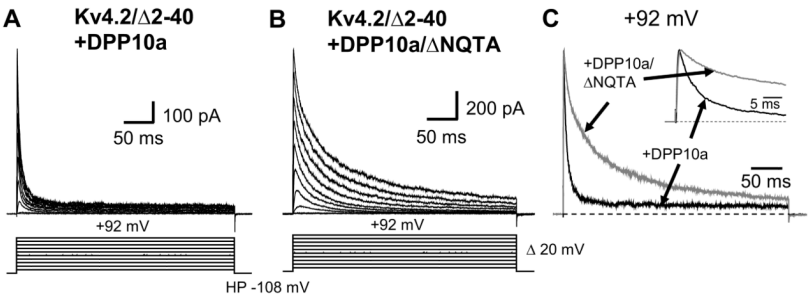

Figure 4. Deletion of the NQTA Residues Also Eliminates DPP10a-mediated Fast Inactivation in Cultured Mammalian Cells

(A) Cell-attached patch recording of Kv4.2/Δ2-40+DPP10a channels expressed in tsA-201 cells. The protocol for step depolarizations is indicated by the voltage trace inset. DPP10a-mediated fast inactivation is similar between tsA-201 cells and oocytes. (B) Deletion of NQTA residues leads to loss of DPP10a-mediated fast inactivation and the observed dramatic slowing of current decay. (C) Normalized current traces at +92 mV illustrate the dramatic slowing of inactivation due to DPP10a N-terminal truncation. Inset shows no change in activation kinetics, indicating that NQTA deletion does not affect Kv4.2-DPP10 association.

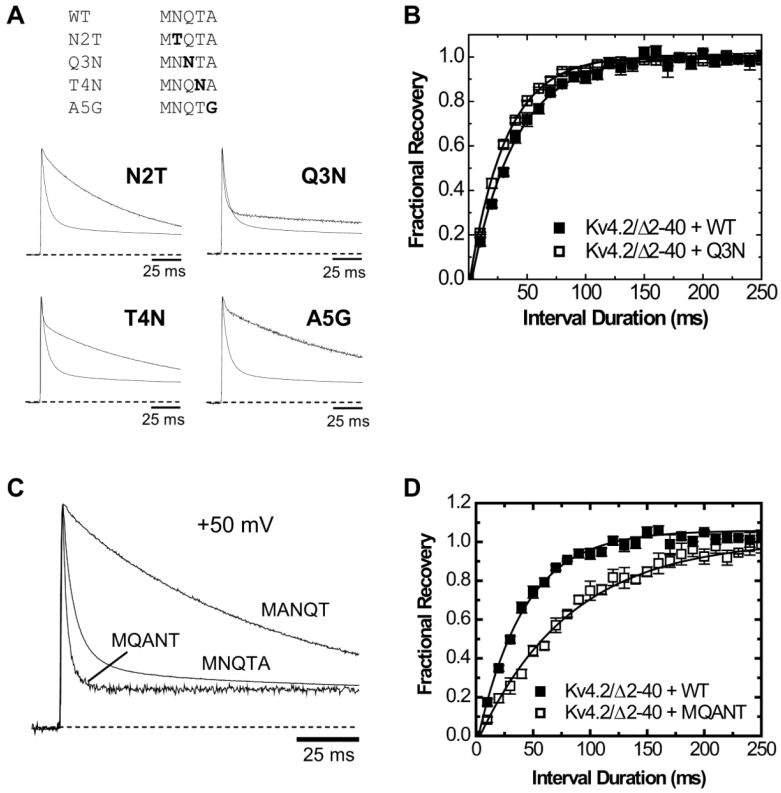

Figure 5. DPP10a-mediated Fast Inactivation is Sensitive to Conservative Substitutions and Sequence Rearrangement of the MNQTA Motif

(A) Normalized whole-ooyte currents at +50 mV from Kv4.2/Δ2-40 channels co-expressed with the indicated DPP10a point mutant. The traces were overlapped with that of normalized Kv4.2/Δ2-40+DPP10a for comparison. (B) The effect of Q3N mutation on the kinetics of recovery from inactivation at −100 mV. The duration of the control pulse was set at 25 ms to allow measurement of recovery from fast inactivation. Lines through the points represent the best fit, assuming a mono-exponential rise. (C) Normalized traces at +50 mV for Kv4.2/Δ2-40 co-expressed with either wild-type DPP10a, the MQANT mutant, or the MANQT mutant. (D) The time course of recovery from inactivation at −100 mV for channels co-expressed with wild-type DPP10a or the MQANT mutant.

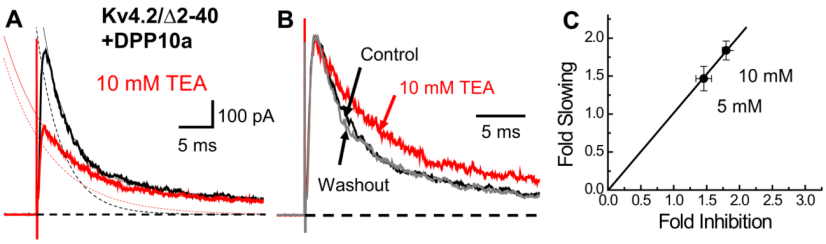

Figure 6. Proportional Inhibition of Peak Current and Slowing of Inactivation of Kv4.2+DPP10a Channels by TEA Suggest Competition between Internal TEA and DPP10a-mediated Inactivation

(A) 10 mM internal TEA reduces Kv4.2/Δ2-40+DPP10a peak current by ~ 46%. Current traces were fitted with 2-exponential functions, and the dashed traces show the decay of the fast component before (black) and after (red) TEA application. Crossing-over of traces illustrates the slowdown of inactivation by internal TEA. (B) TEA-induced slowdown of inactivation, compared by overlapped normalized traces. Both the current inhibition and slowing of inactivation are reversed by washout. (C) Proportionality of fold inhibition and fold inactivation slowing by internal TEA. TEA (5 and 10 mM) was tested for potency in current inhibition and slowing. A direct proportionality is indicated by the identity line drawn, which indicates a 1:1 ratio between fold slowing and fold inhibition. Numbers indicate TEA concentration.

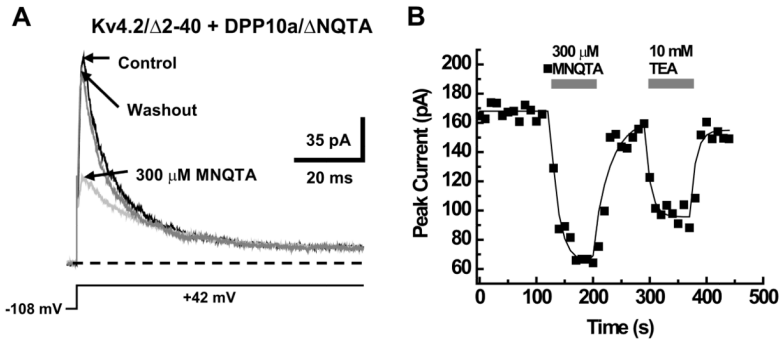

Figure 7. MNQTA Peptide Reversibly Inhibits Kv4.2/Δ2-40 Channel Associated with DPP10a/ΔNQTA

(A) Outward currents at +42 mV mediated by Kv4.2/Δ2-40 channels co-expressed with DPP10a/ΔNQTA. Traces show the reversible suppression of peak current by 300 μM MNQTA peptide application. (B) Timeline of a representative experiment showing the effect of internal perfusion of MNQTA peptide and TEA. Shaded bars indicate the duration of the applications.

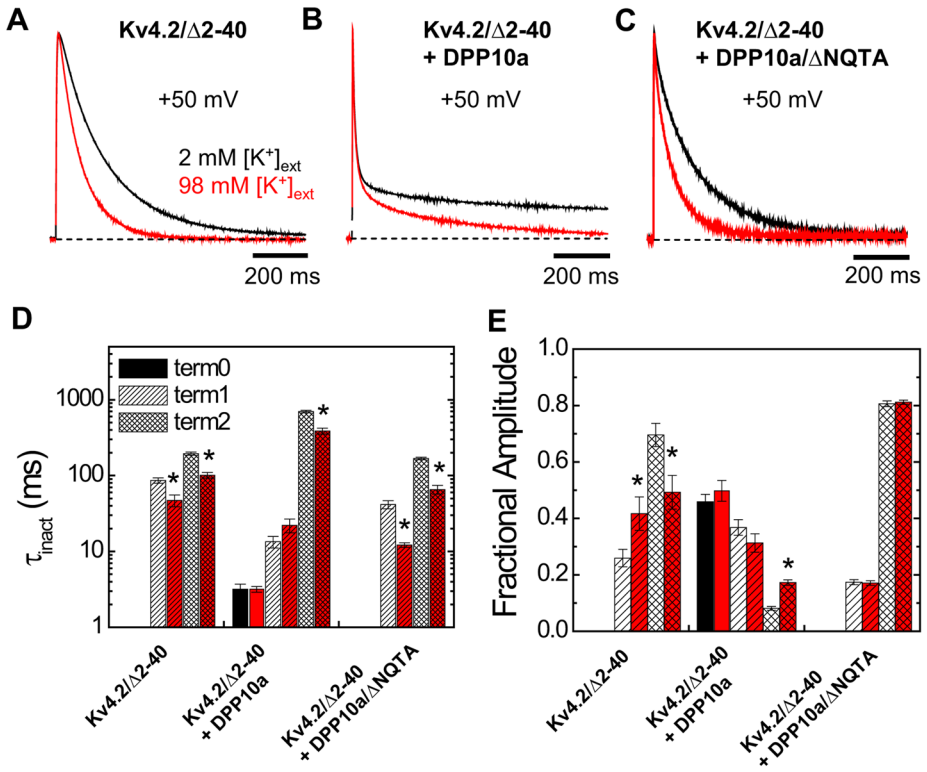

Figure 8. External K^+ Does Not Affect DPP10a-mediated Fast Inactivation

Outward currents at +50 mV from oocytes injected with cRNAs for (A) Kv4.2/Δ2-40, (B) Kv4.2/Δ2-40 and DPP10a, and (C) Kv4.2/Δ2-40 and DPP10a/ΔNQTA. Pulses were repeated after external K^+ concentration was increased from 2 mM to 98 mM by replacing equivalent molar concentrations of Na^+. Note that the fast component of inactivation for Fig. 7B is not affected by elevated K^+, whereas the slow components are dramatically different. Inactivation of currents in Figs. 7A and 7C are markedly accelerated by the ion manipulation. (D) Quantitation of time constants for inactivation at +50 mV for the channels under study. (E) Quantitation of fractional amplitudes for inactivating components at +50 mV. Red bars and traces represent results from 98 mM external K^+; black bars and traces, 2 mM external K^+. Asterisks indicate statistical significance for the value under elevated $[K^+]_{ext}$ with $p < 0.05$.

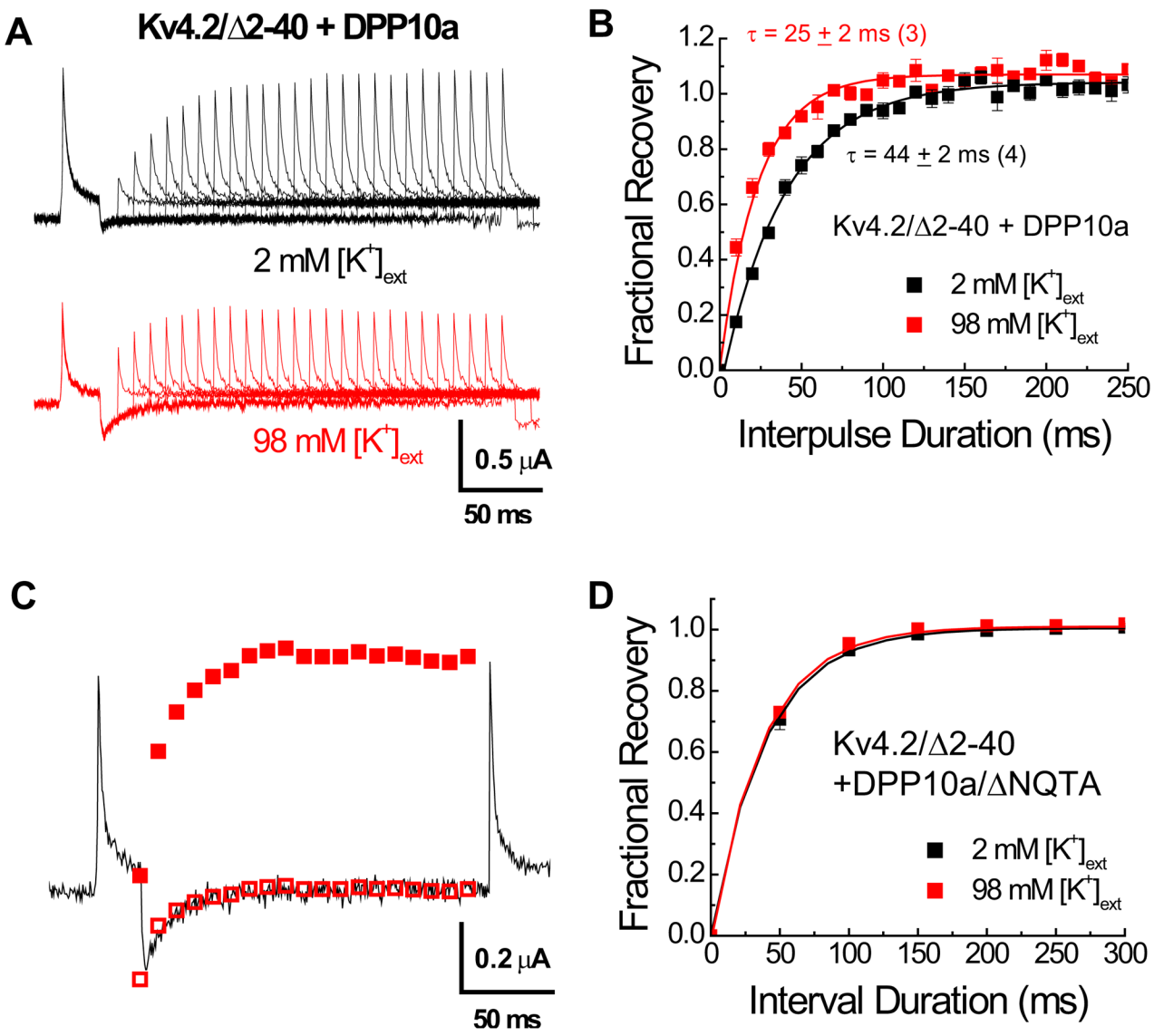

Figure 9. Elevated External K^+ Concentration Accelerates Recovery from MNQTA-dependent Fast Inactivation

(A) Representative traces of Kv4.2/Δ2-40+DPP10a currents elicited by a two-pulse protocol with external K^+ at 2 (black) or 98 (red) mM concentrations. After inactivating channels with +50 mV depolarizing pulse for 25 ms, recovery at −100 mV membrane potential was checked by a second pulse to +50 mV. Peak current returns more rapidly in elevated $[K^+\}_{ext}$. (B) Time course of recovery from inactivation is significantly faster in 98 mM than in 2 mM $[K^+]_{ext}$. The lines represent single exponential fits to the data. (C) The kinetics for recovery from inactivation matches that of channel closing. A representative trace for a two-pulse experiment in 98 mM $[K^+]_{ext}$ is overlapped with the data points of the peak recovered current, before (closed red symbols) and after the values were vertically offset and normalized to the tail current. Amplitude of the tail current at the end of the first pulse was determined by extrapolations of monoexponential fits. (D) Recovery from inactivation of Kv4.2/Δ2-40 channels coexpressed with DPP10a/ΔNQTA is unaffected by increasing $[K^+]_{ext}$.

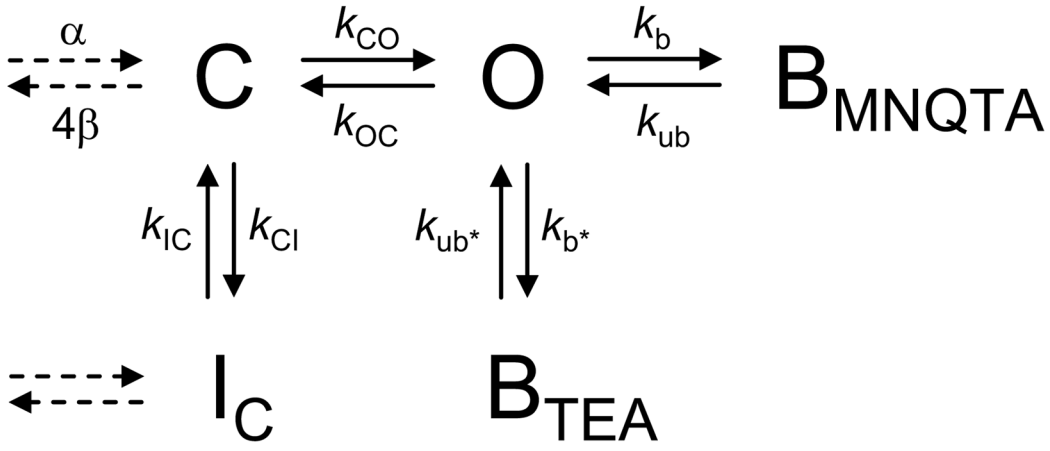

Figure 10. Kv4 inactivation gating and open-state block by MNQTA ID and TEA

Simplified state diagram showing the closed (C), open (O), and closed-inactivated (I_C) states. We hypothesize that during a prolonged depolarization, Kv4 channels coexpressed with DPP10a or DPP6a open and are transiently blocked by the MNQTA peptide (B_{MNQTA}). The internal TEA competes with MNQTA peptide for the open channel by forming the B_{TEA} state, with rapid on- and off-rates. The occupancy of either B_{MNQTA} or B_{TEA} states impairs the ability of Kv4 channels to close and ultimately accumulate in the I_C state, thought to be the absorbing inactivated state of Kv4 channels.[33], [34] Pairs of arrows represents transitions between states with their respective forward and reverse rates. Dashed arrows indicate transitions to closed and closed-inactivated states relatively distant from the open states, which were removed for simplification.